

POLAR3D: Augmenting NASA’s POLAR Dataset for Data-Driven Lunar Perception and Rover Simulation

Bo-Hsun Chen, Peter Negrut, Thomas Liang, Nevindu Batagoda, Harry Zhang, Dan Negrut

Abstract—We report on an effort that led to POLAR3D, a set of digital assets that enhance the POLAR dataset of stereo images generated by NASA to mimic lunar lighting conditions. Our contributions are twofold. First, we have annotated each photo in the POLAR dataset, providing approximately 23 000 labels for rocks and their shadows. Second, we digitized several lunar terrain scenarios available in the POLAR dataset. Specifically, by utilizing both the lunar photos and the POLAR’s LiDAR point clouds, we constructed detailed obj files for all identifiable assets. POLAR3D is the set of digital assets comprising of rock/shadow labels and obj files associated with the digital twins of lunar terrain scenarios. This new dataset can be used for training perception algorithms for lunar exploration and synthesizing photorealistic images beyond the original POLAR collection. Likewise, the obj assets can be integrated into simulation environments to facilitate realistic rover operations in a digital twin of a POLAR scenario. POLAR3D is publicly available to aid perception algorithm development, camera simulation efforts, and lunar simulation exercises.

I. INTRODUCTION

A. Motivation

Renewed interest in lunar exploration is on the rise, driven by the Moon’s potential as a staging ground for missions to more distant celestial bodies like asteroids or Mars. The rate of Moon-focused missions has accelerated, with countries like the U.S., China, India, Russia, and Japan either having completed lunar landings or planning to do so by early 2024. Simulation is critical to the success of these missions since testing in lunar conditions is impractical. The gravitational pull, lighting conditions, terramechanics, and content of the lunar landscape are difficult to reproduce on Earth. This requires increased reliance on simulation environments, see [1], [2], [3], [4], [5]. In simulation, one can easily synthesize and test perception, planning, and controls solutions. Simulation can reduce costs and time to

*This work was supported in part by NASA under project SBIR 80NSSC22PB163.

All authors are with the Simulation-Based Engineering Lab, University of Wisconsin-Madison, Madison, WI-63706, USA {bchen293, pnegrut, thomas.liang, batagoda, hzhang699, negrut}@wisc.edu

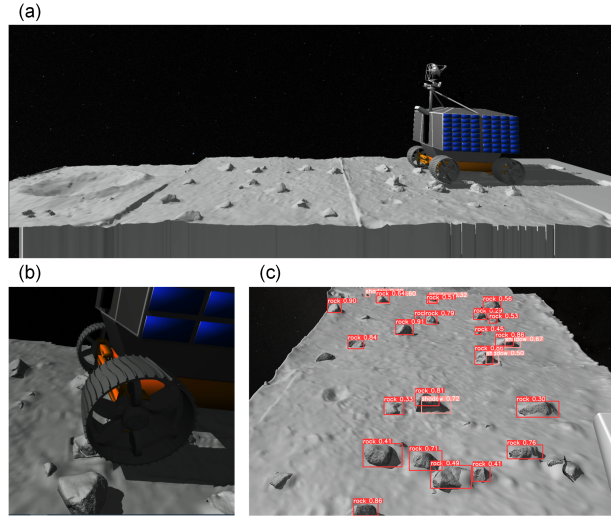


Fig. 1: Illustrations of Viper traversing digitized terrains of the POLAR dataset from right to left when it was running over a responsible rock in POLAR3D. (a) Third-person view from the left side, (b) left-front-wheel-attached camera observing the interaction between the wheel and the terrain, and (c) front-end camera detecting rocks and shadows by YOLOv5 for hazard avoidance.

market, and can be used to generate ground-true labels automatically.

This contribution is motivated by the observation that the task of camera-enabled perception on the Moon is different than the analog task on Earth. Differences arise because camera images from the Earth and Moon have distinct qualitative differences. The lunar surface is covered in lunar regolith, which is a low albedo and retro-reflective material that strongly influences the reflectivity of the lunar surface. The lack of atmospheric scattering and the nature of the lunar regolith are the primary factors dictating the Moon lighting conditions that lead to hard lighting resulting in long shadows, oblique angles of sunlight, and high dynamic range conditions due to the contrast between shadowed and illuminated regions. However, the most outstanding phe-

nomenon caused by interactions of light with the lunar surface is the opposition effect, which is the apparent increase in brightness noted when one observes the lunar surface from the direction of illumination (Sun). The primary reason for the opposite effect is shadow hiding, the phenomenon where all shadows disappear when the viewing and illumination directions are very close [6].

Against this backdrop, in an attempt to spur algorithm development in Computer Vision (CV) for lunar environments, NASA produced and made publicly available the *Polar Optical Lunar Analog Reconstruction (POLAR)* dataset [7], which contains images crafted on Earth to replicate the visual perception conditions of polar lighting on the Moon. The POLAR’s 2500 high dynamic range (HDR) stereo images belong to 13 terrain scenarios that seek to capture both the lighting conditions and the topology of typical lunar landscapes in relation to the size and scattering distribution of rocks, size of fresh craters, etc. Our effort was motivated by a desire to augment NASA’s POLAR dataset with digital assets that assist CV experts interested in improving lunar perception algorithms anchored by data-driven approaches.

B. Contribution

In this work, we have used data in the POLAR dataset to generate digital assets that facilitates the training, testing, and performance evaluation of machine learning algorithms for lunar perception. In a scenario digitization step, we used the LiDAR point clouds of the ground and rocks of each POLAR scenario to manually generate geometric meshes of all assets in each scenario. And, in a labeling step, we manually generated bounding boxes of approximately 23 000 rocks and their shadows in all of the 2500 pairs of POLAR HDR images, thus providing ground-truth for CV algorithms that draw on Machine Learning. As a demonstration of the utility of this labeling and digitization effort, we: (i) carried out both camera simulation and ground vehicle dynamics simulation in POLAR digital twins; and (ii) used the rock/shadow labels to train visual perception algorithms for lunar visual perception conditions.

To the best of our knowledge, this is the first effort to label the photos and digitize the terrains in the POLAR dataset. The main contributions of this paper are as follows:

- We established *POLAR3D*, a publicly available dataset that includes bounding box labels (in YOLO format) for rocks and their shadows, and mesh files of all the separated ground and rocks of the 13 terrain scenarios in the POLAR dataset. POLAR3D

is publicly available in GitHub [8] for unfettered use.

- Using the POLAR3D digital twins, we can synthesize at will labeled photorealistic lunar images via camera simulation and subsequently use them to train and test vision perception algorithms.
- The digitized terrains available in POLAR3D are the digital twins of the POLAR terrains. Beyond being useful for CV tasks, we use the digital terrains to run rover mobility simulations in which one can test in real time perception algorithms at work. Our demo video shows the VIPER rover [9] crossing several digitized POLAR terrains and running over rocks, with a front-end virtual camera detecting rocks via YOLOv5 for hazard avoidance.

C. Related Work

Several widely used labeled datasets, composed of *real-world* photos, are available to benchmark visual perception algorithms [10], [11], [12]. Notably, the *Cityscapes* and *KITTI* datasets are widely employed in autonomous vehicle development [13], [14]. These datasets contain images captured by cameras mounted on cruising cars and encompass various elements, including pedestrians, vehicles, street scenes, and buildings. However, these datasets focus on urban scenarios and are not fit for space exploration perception training.

Several datasets have been curated for extraterrestrial conditions, e.g., the one associated with Mt. Etna, in Sicily, which was deemed a good analogue in terms of soil properties and appearance to Martian conditions [15]; the POLAR dataset [7], which contains 2500 stereo HDR unlabeled images; the Artificial Lunar Landscape Dataset [16], which contains 9766 synthetic, computer generated images of rocky lunar landscapes; Deep Mars [17], which provides an utility for searching a database of more than 22 million pictures of actual Martian landscapes; and MADMAX [18], which is analogous to the POLAR dataset but contains sensor data recorded during a suite of experiments in the Moroccan desert. The information available in POLAR3D is different in two regards: (i) it provides labels on assets associated with images carefully crafted to resemble lunar environments; and, (ii) it opens the door to generating on demand lunar images as soon as one has a camera simulator. We will demonstrate (i) by training our own object detection algorithm on POLAR images using the POLAR3D labels. For (ii), we will demonstrate a simulation of a rover moving in a digital twin world while engaging in perception operations that can be validated against ground-truth data.

II. POLAR3D COMPONENTS

The starting point of this effort was the POLAR dataset, which was set up by NASA using a lunar analog terrain in a sandbox populated with rocks and mild negative and positive obstacles [7]. The terrain and rocks were covered with powdery and fine sand called regolith simulant. A tungsten-halogen spotlight simulated the Sun. This setup replicated the nature of sunlight at a very low elevation angle at the poles, the rugged terrain, and the reflectance of the regolith surface on the Moon.

A. Image annotation

We manually produced bounding boxes to label all POLAR rocks and their shadows. The labels come into play in training data-driven perception algorithms. Object detection is important since large rocks would obstruct the rover's path, and medium and small rocks might damage the wheels and chassis. By the same token, shadows help estimate the Sun's location, which is vital for rover navigation planning, energy harvesting, and camera sensor orientation.

Around 23,000 rocks and shadows were labeled. The parameters within each configuration include the terrain ID, stereo camera position (A, B, or C), rover light status (on or off), Sun azimuth in degrees (no, 30, 180, 270, or 350), camera index in the stereo camera (left or right), and exposure time in milliseconds (32, 64, 128, 256, 512, 1024, or 2048). Above, "no" means no Sun was emulated. Each POLAR photo is associated with a combination of these parameters. Since some of the variables overlapped from photo to photo, the labels for the rocks and shadows remained the same for batches of images. For example, positions of labels were not changed by the exposure time, so an image with exposure time of 32 ms would have the same labels as one with 64, 128, etc. By the same token: different rover light statuses have the same rock and shadow labels; same camera positions with different Sun azimuths have the same rock labels but different shadow labels; the left and right camera views have similar, but not identical, rock and shadow label positions when the other parameters are identical. These observations reduced the labor of labeling the rocks and shadows.

The labeling was done using *labellmg* [19]. First, the left stereo photo of a terrain with rover light OFF was manually labeled. Photos sharing the same settings but varying in exposure time reused the metadata, potentially omitting shadow labels in low-exposure images due to reduced visibility. This label file was also replicated and adjusted for photos from the right camera with similar rock and shadow positions. Then, this label file was

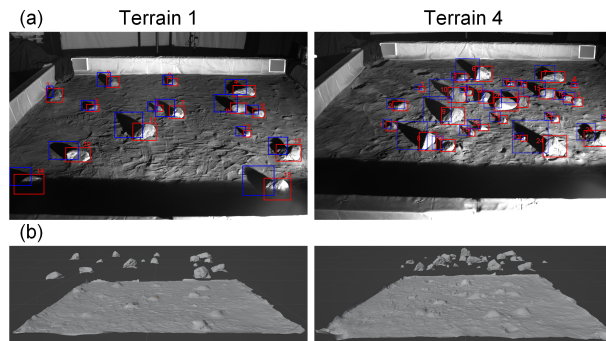


Fig. 2: Illustrations of (a) rock (red) and shadow (blue) bounding box labels and (b) separated meshes of rocks and the ground in the POLAR3D dataset, where the rock meshes are floating over the ground for illustration.

replicated for other photos of different Sun azimuths, with only changing the shadow labels. Thereafter, these label files were replicated for the photos with rover light ON by just fine-tuning the bounding box positions due to on-site hardware setup bias. With this, the labeling of photos from a stereo camera position (A, B, or C) was done, and the procedure was repeated for the other two stereo camera positions to finish the terrain. The same procedure was applied for all of the 13 terrain scenarios in the POLAR dataset. The results were saved in YOLO format as txt, see Fig. 2a for an example.

B. Mesh construction of the ground and rocks

In addition to the photo annotations, POLAR3D includes the mesh obj files of the rocks and the ground for each of the 13 POLAR terrain scenarios. Locating rocks and generating surface meshes was carried out in MATLAB, based on the point cloud data in the POLAR dataset [7]. For each terrain scenario, the two point clouds scanned from the camera positions A and C were inversely transformed back to the sandbox coordinates (where +X: Sun azimuth 0 deg, +Y: Sun azimuth 90 deg, and +Z: upward relative to the sandbox). Subsequently, the positions and orientations of the two point clouds were manually coarse-aligned with each other and located at the sandbox center. Finally, for each rock in the terrain, the positions of the two point clouds were further locally fine-aligned to recover the rock shape, and the X, Y, and Z coordinate ranges forming a bounding cuboid of the rock were manually identified by the annotator.

After locating all the rocks of the terrain, the aligned point clouds of each rock were separated from the ground. Point clouds of the separated rocks and the ground were then converted into meshes using the

Poisson method [20]. The results were stored in obj files, see Fig. 2b for an example.

III. USE CASES

This section discusses three POLAR3D-enabled use cases: object detection using a neural net (NN); generation of synthetic images on demand and assessing their quality for use in perception tasks; and simulation of a rover operating on digitized terrains.

A. Case Study I: Training visual perception algorithms

Bounding box labels of the rocks and shadows were used to train the visual object detection NN YOLOv5. The image annotations in POLAR3D were divided into 816 training photos and 408 testing photos by different exposure time. YOLOv5 was trained via transfer learning to detect rocks and shadows based on the pre-trained model weights of YOLOv5s. And, YOLOv5 was trained and validated both on the training data for 200 epochs with choosing the best weights to use. Then, YOLOv5 trained on real photos was tested on the testing real and synthetic images, as shown in Figure 3. The results are summarized in Table I, where for rock detection we report a triplet of numbers: mean average precision (mAP) for intersection over union (IOU) at threshold 0.5, $mAP@0.5$; mAP over several thresholds, from 0.5 to 0.95, $mAP@[0.5:0.95]$; and IOU_{mean} value. An arrow pointing up in the first row means higher values are better; an arrow down (as shown next to IPD, to be discussed shortly) means lower values are better.

In Table I, the “Train” column, showing Real, Disney (to be discussed shortly), and Hapke (to be discussed shortly), indicates how the object detection NN was trained. In **Case Study I** the focus is on “Real”, which indicates that actual POLAR images are used for training. The row “Eval” indicates what POLAR images were evaluated and used for rock detection by our NN. These images can be Real, Disney, and Hapke. In **Case Study I** the focus is on “Real”, which indicates that actual POLAR images are passed to the NN to assess how astute it is in identifying the rocks in the images. The cornerstone of this effort to assess the quality of the object detection NN is the set of POLAR3D labels – without them, one could neither train nor assess the quality of the YOLOv5 NN. Please note that the values 0.975 / 0.764 / 0.853 are high, indicating that the NN does a good job in recognizing rocks in POLAR images.

B. Case Study II: Lunar image synthesis

The second case study discussed is motivated by the following question: if I generate synthetic camera images, can I use them to train a perception algorithm that

works well on rovers operating on Moon? The ability to generate synthetic images is important since at 2500, the number of images in the original POLAR dataset is relatively small. The goal is to use Computer Graphics techniques to generate on demand synthetic images that are qualitatively similar to what a camera would register on the Moon. Since these actual lunar images are missing, the POLAR images provide the proxy for what lunar images should look like. POLAR3D enables this task of generating on demand labeled lunar images. Since the digital assets in POLAR3D contain meshes for the terrain and the rocks present in all POLAR images, one can draw on any camera simulator to produce synthetic images on demand. Here, we use the Chrono::Sensor camera simulator [21], [22] to produce these synthetic lunar images. Chrono::Sensor simulates high-fidelity cameras for photorealistic image synthesis based on a bi-directional reflectance distribution function (BRDF) and physically-based ray-tracing rendering [21], [22]. To date, we only digitized terrain scenarios 1, 4, and 11; the process of digitizing the remaining ten scenarios is under way.

To build synthetic images, the POLAR3D terrain meshes were placed in the system, and appearance material parameters, e.g., color, metalness, roughness, which are needed in the BRDF, were heuristically set. The simulated Sun, rover light, and cameras were set up in Chrono to take left & right pictures. White point lights without spatial attenuation were set as the sunlight and rover light in simulation. The light intensity ratio of the Sun to rover light was informed by values in the POLAR dataset setup. The locations of sunlight, rover light, and cameras were also set according to the POLAR dataset. Subsequently, images were synthesized by the Chrono virtual camera. To that end, the Disney and Hapke BRDF models were used to synthesize images using the POLAR3D assets. The Disney model, proposed by the Walt Disney Animation Studios, is commonly used to synthesize high-fidelity photorealistic rendering with physically-based ray-tracing in Computer Graphics [23], [24]. The Hapke model was built by design for lunar environments [25], [26], [27]. The Disney-generated, Hapke-generated, and real images were subsequently used in an object detection task that involved YOLOv5. Rock detection results of YOLOv5 trained by real photos and tested on images synthesized by the Disney and Hapke models, respectively, are shown in Fig. 3 and Table I.

While the Case Study I pertain exclusively to the entry 0.975 / 0.764 / 0.853 (called entry R1C1, i.e., row 1 and column 1 of the table), Cast Study II is associated with

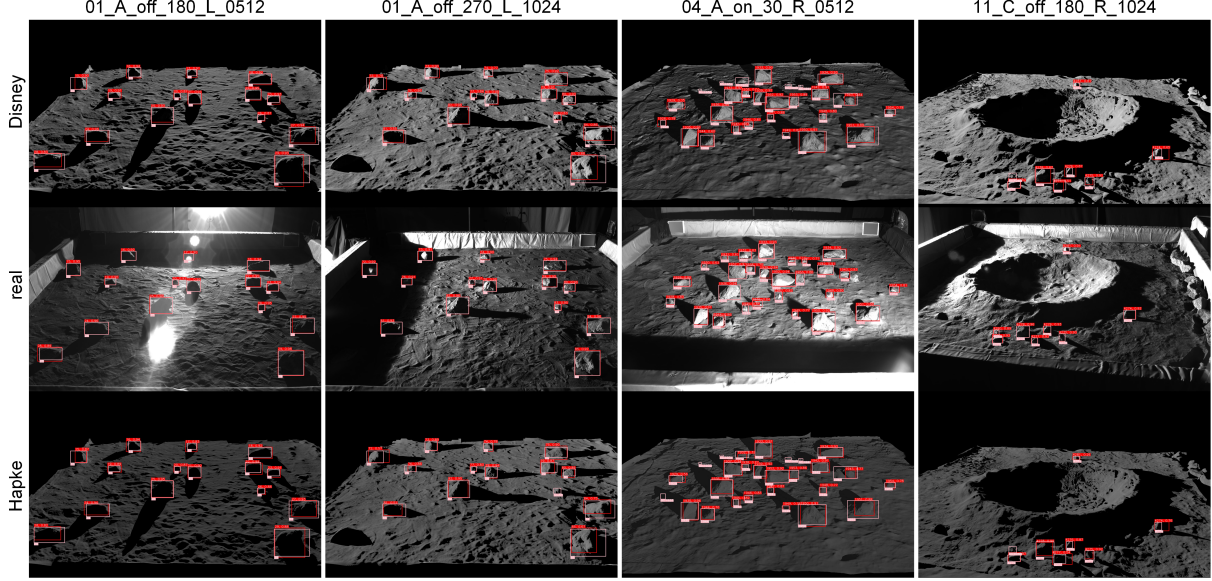


Fig. 3: Illustration comparison of rock detection among real (2nd row), Disney-model-synthesized (1st row), and Hapke-model-synthesized (3rd row) images judged by YOLOv5 trained on real photos. The configuration parameters above each column are represented as: [terrain ID]_[stereo camera position]_[rover light status]_[Sun azimuth]_[Left/Right camera]_[exposure time]. Pink boxes are ground-truth with rock indices, and red boxes are predictions.

TABLE I: Comparison of YOLOv5 rock detection performance results.

Train\Eval	\uparrow mAP@0.5 / mAP@[0.5:0.95] / IOU _{mean}			\downarrow IPD	
	Real	Disney	Hapke	$\ $ Real - Disney $\ $	$\ $ Real - Hapke $\ $
Real	0.975 / 0.764 / 0.853	0.650 / 0.306 / 0.590	0.560 / 0.253 / 0.532	0.2632	0.3211
Disney	0.651 / 0.330 / 0.538	0.913 / 0.818 / 0.899	0.832 / 0.670 / 0.854	0.3606	0.3161
Hapke	0.658 / 0.309 / 0.533	0.907 / 0.738 / 0.878	0.906 / 0.800 / 0.900	0.3452	0.3669

all the other entries. For instance, entry R2C2 captures the performance of the YOLOv5 object detection NN when the NN was trained with synthetic data produced with the Disney model, and the inference to assess to quality of the NN was done via Disney images as well. Similarly, the R2C3 entry provides results for the YOLOv5 NN when it was trained on Disney lunar images but then the NN’s performance was assessed in conjunction with synthetic lunar images generated with the Hapke BRDF. One can notice a significant degradation of YOLOv5’s performance when it trained with POLAR images and then used to identify rocks in synthetic images generated with the Hapke model – the average IOU score is 0.532. In other words, if one simulates the operation of a rover moving in a lunar environment and deploys an object detection NN trained with POLAR images, the NN will do a poor job at picking up rocks as the rovers moves around in simulation (see Case Study III). The reverse is true as well, unfortunately: the 0.533 value suggests that a NN

trained in Chrono using synthetic images generated with the Hapke renderer will do poorly if deployed on an actual rover on Moon (assuming that POLAR images are a good proxy for the actual lunar environment, which may or may not be the case). One should note that the YOLOv5 NN does well when it is asked to do object detection on images that belong to the same class with the ones used for training – see IOU scores on the diagonal – 0.853, 0.899, and 0.900.

Case Study II highlights the fact that the POLAR3D digital assets allow one to produce synthetic images as soon as he/she has access to a camera simulator. Note that whether the synthetic images are or aren’t good proxies for the real images does not depend on POLAR3D assets. Rather, this is controlled by the renderer used (here Chrono::Sensor), and the material properties chosen for the POLAR3D assets (reflectivity, metalness, etc.) Finally, the last two columns in Table I contain numbers associated with the *instance performance difference* (IPD) index [28], which provides more

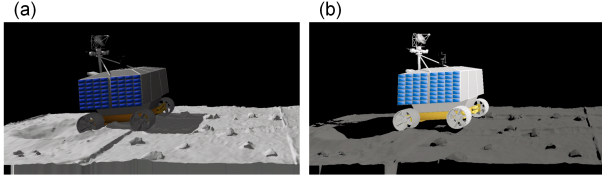


Fig. 4: Different rendering modes from the (a) Disney and (b) Hapke models.

fine-tuned information tied to the statistical similarity of sets of images, e.g., real images vs. Hapke images, when the NN is trained using real, Disney, or Hapke images, respectively. IPD can be regarded as an error, and small values are desired. For details, see [28].

C. Case Study III: Rover operation in digital worlds

This case study highlights how the POLAR3D assets facilitate model-based synthesis for elements of a robot autonomy stack. Specifically, the digital assets created enable the creation of a virtual lunar world. In this case, since the digitization effort thus far produced only three of the 13 terrain scenarios available in POLAR, we combined these three patches of lunar scenario analogs into one “virtual world” and subsequently proceeded to run simulations in it. The POLAR terrain scenarios stitched together were 4, 1, and 11. Subsequently, we used Chrono to simulate the motion of the VIPER rover model operating in this digital world. The terrain was considered deformable and represented via the soil contact model (SCM) terramechanics [29] to capture the interaction between the rover and terrain – while the rover moved in the digital world, virtual cameras were registering images. The cameras were added next to the four wheels of the vehicle to observe at close range the terramechanics between the wheel and terrain. For hazard avoidance, a virtual camera was mounted on the front-end of VIPER, and the images produced by the virtual camera were passed to YOLOv5 for rock and shadow detection. The Deep Star Map HDR image was used as sky background [30].

This setup allows one to test perception, planning, and controls algorithms in a model-based and data-driven design framework. To that end, in addition to the POLAR3D digital assets, one needs a simulator, which in this case study was Chrono. This choice was convenient since Chrono handles in a one framework sensor, vehicle, and terramechanics simulation.

IV. DEMONSTRATION

The media file uploaded shows a VIPER simulation as the rover traverses a deformable lunar terrain with

rocks and a crater. Images from the virtual cameras are shown in Fig. 1. The videos show VIPER traversing three terrains – 4, 1, and 11 – as it clears four rocks and a crater. Figure 1a shows a third-person camera view. Figure 1b shows the same instance from the left-front-wheel-attached camera when VIPER was running over a rock. Since SCM deformable terrain provides accurate terramechanics simulation, the rover can be tested for different soil parameters or wheel topologies. Lastly, Fig. 1c shows the front-end camera with YOLOv5 detection result, which can detect rocks and shadows while it moves over the terrain. This simulation setup enables the testing of perception, planning, and control algorithms in simulation under different lighting, camera angle, and environmental conditions. Finally, Fig. 4 highlights the difference between the Hapke and Disney BRDFs. The Hapke model, designed for lunar environments, rendered a darker and longer shadow of VIPER and brighter back-scatter of the terrain.

V. CONCLUSIONS

We report on an effort that led to *POLAR3D*, a set of digital assets that enhances NASA’s POLAR dataset of stereo images created to mimic lunar lighting and environment conditions [7]. *POLAR3D* includes (i) manually labeled bounding boxes of rocks and their shadows for approximately 23 000 rocks that appear in the 2500 stereo images of the POLAR dataset; and (ii) manually generated meshes of the ground and rocks that provide digital twins for some of the POLAR scenarios. Work is under way to digitize all the remaining POLAR terrain scenarios. We showcased the use of the *POLAR3D* assets in three tasks: training of a YOLOv5 object detection NN that was carried out using the newly defined labels; ability to generate at will synthetic photographs in the image of the POLAR terrain scenarios by virtue of having produced meshes required to generate digital twins; and, a VIPER simulation as the rover operates in a virtual world stitched together from digital twins of terrain scenarios selected from the POLAR dataset. Further improvements pertain to pixel-level image annotations for semantic segmentation, automatically generating ground-true shadow labels in synthetic images, and the use of pretrained NNs to expedite the digitization of the remaining POLAR terrain scenarios. The latter would alleviate some of the heavy burden of manually generating the digital twin of a POLAR terrain scenario.

REFERENCES

- [1] S. M. Parkes, I. Martin, M. Dunstan, and D. Matthews, "Planet Surface Simulation with PANGU," in *Space OPS 2004 Conference*, Montreal, Quebec, Canada, May 2004.
- [2] R. Brochard, J. Lebreton, C. Robin, K. Kanani, G. Jonniaux, A. Masson, N. Despré, and A. Berjaoui, "Scientific image rendering for space scenes with the SurRender software," *arXiv:1810.01423*, 2018.
- [3] M. Allan, U. Wong, P. M. Furlong, A. Rogg, S. McMichael, T. Welsh, I. Chen, S. Peters, B. Gerkey, M. Quigley, M. Shirley, M. Deans, H. Cannon, and T. Fong, "Planetary Rover Simulation for Lunar Exploration Missions," in *IEEE Aerospace Conference (AERO)*, Big Sky, Montana, USA, 2019, pp. 1–19.
- [4] M. G. Müller, M. Durner, A. Gaweł, W. Stürzl, R. Triebel, and R. Siegwart, "A Photorealistic Terrain Simulation Pipeline for Unstructured Outdoor Environments," in *IEEE/RSJ International Conference on Intelligent Robots and Systems (IROS)*, Prague, Czech Republic, Sep. 2021, pp. 9765–9772.
- [5] M. Sewtz, H. Lehner, Y. Fanger, J. Eberle, M. Wudenka, M. G. Müller, T. Bodenmüller, and M. J. Schuster, "URSim - A Versatile Robot Simulator for Extra-Terrestrial Exploration," in *IEEE Aerospace Conference (AERO)*, Big Sky, Montana, USA, 2022, pp. 1–14.
- [6] A. Kuzminykh, "Physically based real-time rendering of the moon," Ph.D. dissertation, Hochschule Hannover, 2021.
- [7] U. Wong, A. Nefian, L. Edwards, X. Buoyssounouse, P. M. Furlong, M. Deans, and T. Fong, "Polar Optical Lunar Analog Reconstruction (POLAR) stereo dataset," *NASA Ames Research Center*, 2017.
- [8] B.-H. Chen, P. Negrut, T. Liang, N. Batagoda, H. Zhang, and D. Negrut, "POLAR3D Dataset," <https://github.com/uwsbel/POLAR-digital.git>, 2023.
- [9] A. Colaprete, D. Andrews, W. Bluethmann, R. C. Elphic, B. Bussey, J. Trimble, K. Zacny, and J. E. Captain, "An overview of the volatiles investigating polar exploration rover (viper) mission," in *AGU fall meeting abstracts*, vol. 2019, 2019, pp. P34B–03.
- [10] G. Neuhold, T. Ollmann, S. Rota Bulò, and P. Kotschieder, "The mapillary vistas dataset for semantic understanding of street scenes," in *Proceedings of the IEEE international conference on computer vision*, 2017, pp. 4990–4999.
- [11] X. Huang, X. Cheng, Q. Geng, B. Cao, D. Zhou, P. Wang, Y. Lin, and R. Yang, "The ApolloScape Dataset for Autonomous Driving," in *IEEE/CVF Conference on Computer Vision and Pattern Recognition (CVPR) Workshops*, Salt Lake City, UT, USA, Jun. 2018, pp. 1067–1073.
- [12] F. Yu, H. Chen, X. Wang, W. Xian, Y. Chen, F. Liu, V. Madhavan, and T. Darrell, "BDD100K: A diverse driving dataset for heterogeneous multitask learning," in *IEEE/CVF Conference on Computer Vision and Pattern Recognition (CVPR)*, June 2020.
- [13] M. Cordts, M. Omran, S. Ramos, T. Rehfeld, M. Enzweiler, R. Benenson, U. Franke, S. Roth, and B. Schiele, "The cityscapes dataset for semantic urban scene understanding," in *Proceedings of the IEEE conference on computer vision and pattern recognition*, 2016, pp. 3213–3223.
- [14] A. Geiger, P. Lenz, C. Stiller, and R. Urtasun, "Vision meets robotics: The KITTI dataset," *The International Journal of Robotics Research*, vol. 32, no. 11, pp. 1231–1237, 2013.
- [15] M. Vayugundla, F. Steidle, M. Smisek, M. J. Schuster, K. Bussmann, and A. Wedler, "Datasets of Long Range Navigation Experiments in a Moon Analogue Environment on Mount Etna," in *International Symposium on Robotics (ISR)*, Munich, Germany, Jun. 2018, pp. 77–83.
- [16] Q. J. Romain Pessia, Genya Ishigami, "Artificial lunar landscape dataset," 2019. [Online]. Available: <https://www.kaggle.com/datasets/romainpessia/artificial-lunar-rocky-landscape-dataset>
- [17] K. Wagstaff, Y. Lu, A. Stanboli, K. Grimes, T. Gowda, and J. Padams, "Deep Mars: CNN Classification of Mars Imagery for the PDS Imaging Atlas," *Proceedings of the AAAI Conference on Artificial Intelligence*, vol. 32, no. 1, 2018.
- [18] L. Meyer, M. Smíšek, A. Fontan Villacampa, L. Oliva Maza, D. Medina, M. J. Schuster, F. Steidle, M. Vayugundla, M. G. Müller, B. Rebele, A. Wedler, and R. Triebel, "The MADMAX data set for visual-inertial rover navigation on Mars," *Journal of Field Robotics*, vol. 38, no. 6, pp. 833–853, 2021.
- [19] Tzutalin, "LabelImg," *GitHub repository*, 2015. [Online]. Available: <https://github.com/tzutalin/labelImg>
- [20] M. Kazhdan, M. Bolitho, and H. Hoppe, "Poisson Surface Reconstruction," in *Proceedings of the Eurographics Symposium on Geometry Processing*, ser. SGP '06. Cagliari, Sardinia, Italy: Eurographics Association, 2006, pp. 61–70.
- [21] A. Elmquist, R. Serban, and D. Negrut, "A Sensor Simulation Framework for Training and Testing Robots and Autonomous Vehicles," *Journal of Autonomous Vehicles and Systems*, vol. 1, no. 2, pp. 021 001–1– 021 001–10, 2021.
- [22] A. Elmquist and D. Negrut, "Modeling Cameras for Autonomous Vehicle and Robot Simulation: An Overview," *IEEE Sensors Journal*, vol. 21, no. 22, pp. 25 547–25 560, 2021.
- [23] B. Burley and W. D. A. Studios, "Physically-based shading at Disney," in *SIGGRAPH*, 2012.
- [24] W. D. A. Studios, "BRDF Explorer," *GitHub repository*, 2012. [Online]. Available: <https://github.com/wdas/brdf>
- [25] H. Sato, M. S. Robinson, B. Hapke, B. W. Denevi, and A. K. Boyd, "Resolved Hapke parameter maps of the Moon," *Journal of Geophysical Research: Planets*, vol. 119, no. 8, pp. 1775–1805, 2014.
- [26] B. Hapke, "Bidirectional reflectance spectroscopy: 1. Theory," *Journal of Geophysical Research: Solid Earth*, vol. 86, no. B4, pp. 3039–3054, 1981.
- [27] —, "Bidirectional reflectance spectroscopy: 6. Effects of porosity," *Icarus*, vol. 195, no. 2, pp. 918–926, 2008.
- [28] B. Chen and D. Negrut, "Instance performance difference (ipd)," Simulation-Based Engineering Laboratory, University of Wisconsin-Madison, Tech. Rep., 2023, <https://sbel.wisc.edu/technicalreports/>.
- [29] A. Tasora, D. Mangoni, D. Negrut, R. Serban, and P. Jayakumar, "Deformable soil with adaptive level of detail for tracked and wheeled vehicles," *International Journal of Vehicle Performance*, vol. 5, no. 1, pp. 60–76, 2019.
- [30] NASA/Goddard Space Flight Center Scientific Visualization Studio, "Deep Star Maps," 2020. [Online]. Available: <https://svs.gsfc.nasa.gov/4851>